RECOGNITION OF THE CONDITION OF CONSTRUCTION MATERIALS USING SMALL DATASETS AND HANDCRAFTED FEATURES

Eyob Mengiste
New York University Abu Dhabi, United Arab Emirates, and Technical University of Berlin, Germany
Email: eyob.mengiste@nyu.edu

Borja Garcia de Soto
New York University Abu Dhabi, United Arab Emirates
Email: garcia.de.soto@nyu.edu

Timo Hartmann
Technical University of Berlin, Germany
Email: timo.hartmann@tu-berlin.de

SUMMARY: We propose using handcrafted features extracted from small datasets to classify the conditions of the construction materials. We hypothesize that features such as the color, roughness, and reflectance of a material surface can be used to identify details of the material. To test the hypothesis, we have developed a pre-trained model to classify material conditions based on reflectance, roughness and color features extracted from image data collected in a controlled (lab) environment. The knowledge learned in the pre-trained model is finally transferred to classify material conditions from a construction site (i.e., an uncontrolled environment). To demonstrate the proposed method, 80 data points were produced from the images collected under a controlled environment and used to develop a pre-trained model. The pre-trained model was re-trained to adapt to the real construction environment using 33 new data points generated through a separate process using images collected from a construction site. The pre-trained model achieved 93%; after retraining the model with the data from the actual site, the accuracy had a small decrease as expected, but still was promising with an 83% accuracy.

KEYWORDS: Image processing, transfer learning, roughness, reflectance, color, CIELab, small datasets

1 INTRODUCTION

Automated construction data processing could improve the efficiency of monitoring of construction progress and quality assurance by enabling efficient quantity calculation, quality monitoring, and detection of defects. Traditional progress monitoring depends on manual site observation and paper-based quantification of works which is prone to error in recognizing quality discrepancies and determining the quantity of work. Moreover, the process is inefficient in terms of time and labor, reducing the ability to complete a project within a given time and budget constraints. According to the PMI publication, for multiple reasons, only 57% and 66% of construction projects are completed within the planned time and budget, respectively (Pulse of the Profession, 2021). Automating inefficient manual data collection and processing practices within the construction industry could enable project managers to work on accurate site observation and measurement information, with increased attention to controlling cost and schedule throughout the construction process (Teizer, 2015).

Recently, extensive research has focused on automated construction data collection and processing to achieve accurate material recognition using sensing systems and machine learning algorithms. Most material recognition methods focus on detecting materials and elements, regardless of their condition (Degol et al., 2016; Dimitrov and Golparvar-Fard, 2014; Maalek et al., 2019). This limits the possibility of understanding the status of a construction site, as the materials themselves undergo significant temporary and permanent changes in appearance. If a construction task is associated with a given material, the status of the task can be determined by tracking the variation (e.g., textural variation) of the material. For instance, a cast-in-place concrete slab can be left unfinished (rough) or may become smooth and reflective after screeding. Both the cast-in-place slab (rough) and the screed (smooth) one have different appearance states or material conditions. In the context of this study, 'material condition' refers to the condition (i.e., appearance) of a given material associated with a given task with the presumption that the condition can be linked to the state of the related task. A certain trade needs to put effort into completing the screeding work on the concrete slab. Therefore, recognizing material conditions increases the understanding of the construction status. Material layers could be rough, while subsequent layers could be relatively smooth, depending on the finishing requirements. Applying each layer on the construction site takes a specific amount of time, cost and effort. Therefore, tracking the detailed conditions of the construction materials can provide a better understanding of the progress of the associated tasks, hence the project. This study addresses previous limitations by using handcrafted features such as the color, roughness, and reflectance of a material surface extracted from small datasets to classify construction materials and used to identify details of the material condition and track the temporary and permanent changes in the appearance of construction materials associated with different construction tasks.

One of the primary challenges in tracking material conditions is the scarcity of comprehensive and labeled data. In general, training supervised machine learning algorithms to track and understand detailed changes in material appearance requires extensive training data. Image libraries, widely used to train material recognition algorithms, can represent the color, shape, or other two-dimensional patterns on the material surface. However, they are not created to provide out-of-surface (i.e., 3D) textural details. Moreover, it is difficult and time-consuming to label images collected from construction sites according to detailed material conditions. One of the reasons for this is that material conditions could be hard to identify manually from an image without referring to the actual construction site.

This study presents a method of recognizing material conditions automatically from a small dataset. The classifier is developed using a dataset generated in a controlled lab environment. Handcrafted features, such as roughness, reflectance and color, are extracted from the laboratory data before the machine learning model is developed. The developed model is transferred to an as-is dataset collected from a real construction environment. In this study, the term 'as-is' represents the state of the construction during the data collection. The outcome of this method is to track detailed variations in the condition of construction materials that have a shortage of labeled datasets.

The rest of this paper is organized as follows: Section 2 identifies gaps in state-of-the-art material recognition research. Section 3 presents the proposed research method, and Section 4 demonstrates the application of the developed method in the construction environment. Section 5 shows the testing results, while Section 6 discusses the contribution of this study to the current state of the art, practical impacts, overall limitations, and recommendations for future work. Finally, Section 7 presents the conclusions.

2 LITERATURE REVIEW

Over the past few decades, material recognition has played an essential role in automating manual activities in construction. This section presents the current state of the art in construction material recognition research.

2.1 Material recognition research in construction

Image-based approaches primarily analyze images and videos using computer vision and image processing techniques. Dimitrov and Golparvar-Fard (2014) proposed a material recognition approach based on the descriptors extracted from color and image filter responses. Based on this work, Han and Golparvar-Fard, (2014) developed an operation-level approach to monitoring construction progress in which the BIM model was back-projected into an as-built point cloud generated from site images to define deviations in progress. When classifying materials in both methods, the size of filters to be applied in extracting features could result in hiding or yielding noisy information regarding the material condition of small elements, such as the edges of slender members or electrical outlet points. Considering texture variation of materials in the construction site to train an algorithm for material recognition increases the level of detail of feature representation. For example, Deng et al. (2020) developed a method to track tile-paving progress in indoor construction. The recognition algorithm was developed to identify tiled areas using an image database with intentionally varying texture, camera perspective and lighting data.

Multiple machine learning algorithms have been used in construction material recognition research. Support Vector Machine (SVM) has been applied in both material recognition and construction progress monitoring research (Deng et al., 2020; Dimitrov and Golparvar-Fard, 2014; Hamledari, McCabe, and Davari, 2017). Deng et al. (2020) and Hamledari et al. (2017) proposed identifying specific materials related to specific tasks to monitor construction progress. Those studies all exploited the illumination response of shiny surfaces to extract patterns of specific materials under consideration. Aside from SVM, researchers have explored several other deep and shallow machine learning algorithms (Ghassemi et al., 2020; Son et al., 2014).

Son et al. (2014) proposed a construction material recognition method using ensemble classifiers, which were comprised of six different classifiers, including Support Vector Machine (SVM), Artificial Neural Networks (ANN), Naïve Bayes (NB), Logistic Regression (LR) and K-nearest Neighbors (KNN). These individual classifiers were trained to classify different materials, such as steel, concrete, and timber. The training data was developed using 250 images, non-uniformly distributed between the three classes. Images were pre-processed and sub-regioned into smaller pixel sizes to maximize training data count. RGB values were converted into HSV color space to reduce the illumination effect in the pixel color attributes. The results showed that ensemble classifiers performed better than single classifiers, regardless of the weather and illumination conditions on the construction site.

Similarly, Ghassemi et al. (2020) proposed a material recognition method for monitoring the progress of automated construction. This method explored Deep Convolutional Neural Network (DCNN) structures, such as Visual Geometry Group (VGG), ResNet, DenseNet, and NASNet mobile. Results demonstrated that the DCNN structures considered performed with an accuracy rate greater than 92%. Son et al. (2014) and Ghassemi et al. (2020) identified illumination and data scarcity as challenges. Son et al. (2014) pre-processed the available data to separate the chrominance and luminance information, and Ghassemi et al. (2020) incorporated data with different illumination orientation conditions during the training. Moreover, Ghassemi et al. (2020) added random outliers to the data to overcome overfitting resulting from the data size.

Although classical machine learning methods achieve good accuracy in material recognition, the conditions that the materials are going through are overlooked. For instance, in Son et al. (2014) and Ghassemi et al. (2020), concrete is simply detected as concrete, regardless of its finishing state. Similarly, timber is only recognized as timber, regardless of its state; yet, timber can be processed and smoothed or raw and rough. Although it is technically feasible to apply a similar approach in detecting detailed construction material conditions, developing a sizable database to represent each construction stage and material condition effectively— and large enough to define patterns using the above-mentioned machine learning models—may be prohibitive in terms of time.

Researchers have proposed transfer learning as a potential approach to achieving a promising accuracy level to classify materials based on their appearance states. The method transfers pre-trained features from a given model as input to another task without pre-training (Weiss, Khoshgoftaar and Wang, 2016). For instance, in

infrastructural material studies, (Gopalakrishnan, Khaitan, Choudhary and Agrawal, 2017) performed a study to detect pavement distress by transferring knowledge from a DCNN trained on a big image dataset. The pre-trained DCNN model features were further evaluated using 1056 local images to achieve a maximum of 87% accuracy. Although transfer learning performs well by sharing knowledge and saving computational time and resources, fine-tuning the model to the desired new purpose still requires a significant amount of data.

Alternative approaches to the data limitation challenge include data augmentation and feature engineering. Most augmentation techniques inflate the available data by artificially creating data instances by applying multiple techniques, including scaling, clipping, shearing, rotating, mixing and convolving existing images (Shorten and Khoshgoftaar, 2019). Data augmentation could overcome challenges related to irrelevant information in the image, such as background or problems related to image distortion. However, it can only simulate the increase in data size with minimal contribution of new information during a feature pattern definition. Training deep neural networks using a small dataset results in a weak generalization of features. This is mainly because features are extracted automatically through the layers of the network, and neural networks generally require a significant amount of data to generalize a pattern with reasonable confidence. Therefore, in the case of a small dataset, handcrafted feature extraction could force the networks to focus on specific features (Das, Arshad, Manjhi, and Thepade, 2020). The following sections describe a selected set of features utilized in the literature to define a material's appearance.

2.1.1 Color features

With several color attribute models proposed in the literature, color is one of the most used object recognition features. The common challenge in extracting descriptors from color information is the dependency of color information on the illumination of the environment (Ebner, 2007). The more stable chrominance characteristics of a material can be computed by converting imagery into relatively illumination-invariant color spaces to help reduce image data dependency upon illumination of the environment. The most widely-used color space to represent a material's chromatic character is Hue Saturation and Value (HSV) (Braun et al., 2020; Quintana et al., 2018). However, HSV color space has limitations in clearly representing differences between materials with monochromatic and achromatic color characteristics, such as concrete (Son et al., 2012). CIELab color space is another alternative color space used to reduce the effect of environmental illumination in construction component recognition and progress monitoring (Hamledari et al., 2017; Mengiste and Garcia de Soto, 2018). However, in some instances, materials appeared to have constant color characteristics throughout different construction states, regardless of the work progress. Therefore, color features are not enough to detect progress and material state.

2.1.2 Surface roughness

Roughness is a measure of out-surface irregularity. It is common in pavement condition classification research which requires laser scanning using infrared-based devices, such as time-of-flight (ToF) cameras or LiDAR scanners (Díaz-Vilariño et al., 2016; Mahmoudzadeh et al., 2019) to extract roughness information. Although roughness is used frequently for pavement classification, the high equipment and operational expenses of accurate depth cameras and laser scanners hinder the use of the feature for regular day-to-day activities in tracking construction progress. As an alternative, researchers have looked at more affordable photogrammetric methods to generate point cloud data (PCD) and experiment with roughness feature extraction. Petitpas et al. (2010) proposed a method for extracting surface roughness from unconstrained image data. In their method, a dense stereoscopic point cloud was developed using photogrammetry. Roughness was calculated based on the root mean square and arithmetic mean of depth, which was measured as a stochastic variation between points and the reference surface.

Petitpas et al. (2010) noted multiple sources of error in these calculations of surface roughness. Most of them were due to filtering procedures to reduce noise caused by mismatched images, which affected roughness estimation quality. This study adopts the method Petitpas et al. (2010) proposed by applying a defined threshold margin to limit the extent of noise around the reference surface.

2.1.3 Surface reflectance

Material reflectance is a spectral property of a material, measured as the ratio of irradiance transmitted through the material to the incident irradiance (Eismann, 2012). Bidirectional Reflectance Distribution Function (BRDF) is the expression of reflectance characteristics demonstrated by emphasizing the amount of multi-directional refraction of illumination from every possible direction toward the surface in focus. Light incoming to a surface

reflects in any random direction; objects placed within close range of one another can inter-reflect. Therefore, identifying the source and original direction of natural light radiation to measure and calculate BRDF accurately is not trivial. Although computer vision and applied optics articles (Cula and Dana, 2004; Kim, Lim, Ahn and Lee, 2018; Chao Liu and Gu, 2014; Marschner, Westin, Arbree and Moon, 2005; Marschner, Westin, Lafortune and Torrance, 2000; Sole, Farup, Nussbaum and Tominaga, 2018; H. Zhang, Dana and Nishino, 2015) have proposed methods for estimating BRDF to approximate reflectance property of materials using laser-emitting devices, the method's applicability to the construction site is limited because the data inputs were collected under heavily controlled conditions.

To replace the utilization of a controlled environment in measuring BRDF, Lai, Liu, Zhao, Zhao and Tan (2020) developed a BRDF simulation model based on experimental results. In their method, optimal model parameters are computed using genetic algorithms, where the parameter fitting of the objective function was performed through empirical data fitting. Therefore, this method depended on data generation under a highly controlled environment, employing a sensitive up-close optical setup such as a scatterometer. Similarly, Erickson, Xing, Srirangam, Chernova and Kemp (2020) and Ohi, Mridha, Hamid, Monowar and Kateb (2021) proposed a method of recognizing objects using up-close visual measurements. Whereas the former uses spectrometry measurements to collect data, multimodal networks are trained to represent various modalities with different groups of SpectroVision datasets. The latter collected up-close microscopic image data to determine the fiber characteristics of textiles samples. Although results obtained from both publications were promising, the size of the training data and the data collection scheme requires up-close spectrometry (approximately 1cm distance) or microscopy, which is limiting for application in a complex construction site. Ce Liu, Sharan, Adelson and Rosenholtz (2010) developed an alternative method that defines color, texture and micro-texture from 2D image-based measurements of parameters such as surface BRDF, object shape and environmental lighting. Although the method achieved only a 44.6% recognition rate, its independence from special requirements such as spectroscopy instrument, close up position during data collection or controlled environment, makes it promising for construction site applications.

The possibility of approximating surface reflectance from image data in construction sites has not yet been sufficiently explored. In this study, a novel method of reflectance measurement is developed. The technique depends on coupled images, where the reflectance is extracted by subtracting one of the images taken under natural illumination from the other set of photos taken under both natural and artificial illumination conditions.

3 THE PROPOSED METHOD

The proposed method (Figure 1) consists of five sections. The first section relates to data generated in a controlled lab environment. The produced data set was pre-processed in the second section to extract the features (color, roughness, and reflectance). The extracted handcrafted features are used to pre-train a material condition classifier in the third section. The fourth section is about the data collection and feature extraction from the actual construction site environment. In the last section, the pre-trained model is transferred to classify actual construction information using the feature data resulting from step four.

3.1 Data collection from the controlled Lab environment

The condition of construction materials is expected to change throughout the course of construction. The changes in the condition of a given set of materials were determined and established in a controlled environment. Three sets of image data were collected to accommodate the requirements of the three features considered (i.e., color, roughness, and reflectance). Figure 5 presents a set of sample images taken in the controlled environment. Each image was captured by focusing on each element with the specific condition and excluding any background objects. For reflectance feature extraction, coupled sets of reference images were collected under natural and artificial illumination conditions in various orientations. Stereoscopic sets of images were taken under natural illumination to capture the roughness characteristics of material surfaces. Finally, to extract color features representing each material condition, a separate set of images with random scale and rotation from different viewpoints under natural illumination conditions ware taken.

3.2 Feature extraction from data collected in the Lab environment

The collected data was transformed into a feature data set used to train the classification algorithm. In this step, the raw image data set collected to represent the material conditions was converted into a training data vector. This

section is divided into three sub-sections, each one elaborating on the detailed process for extraction of reflectance, roughness, and color features.
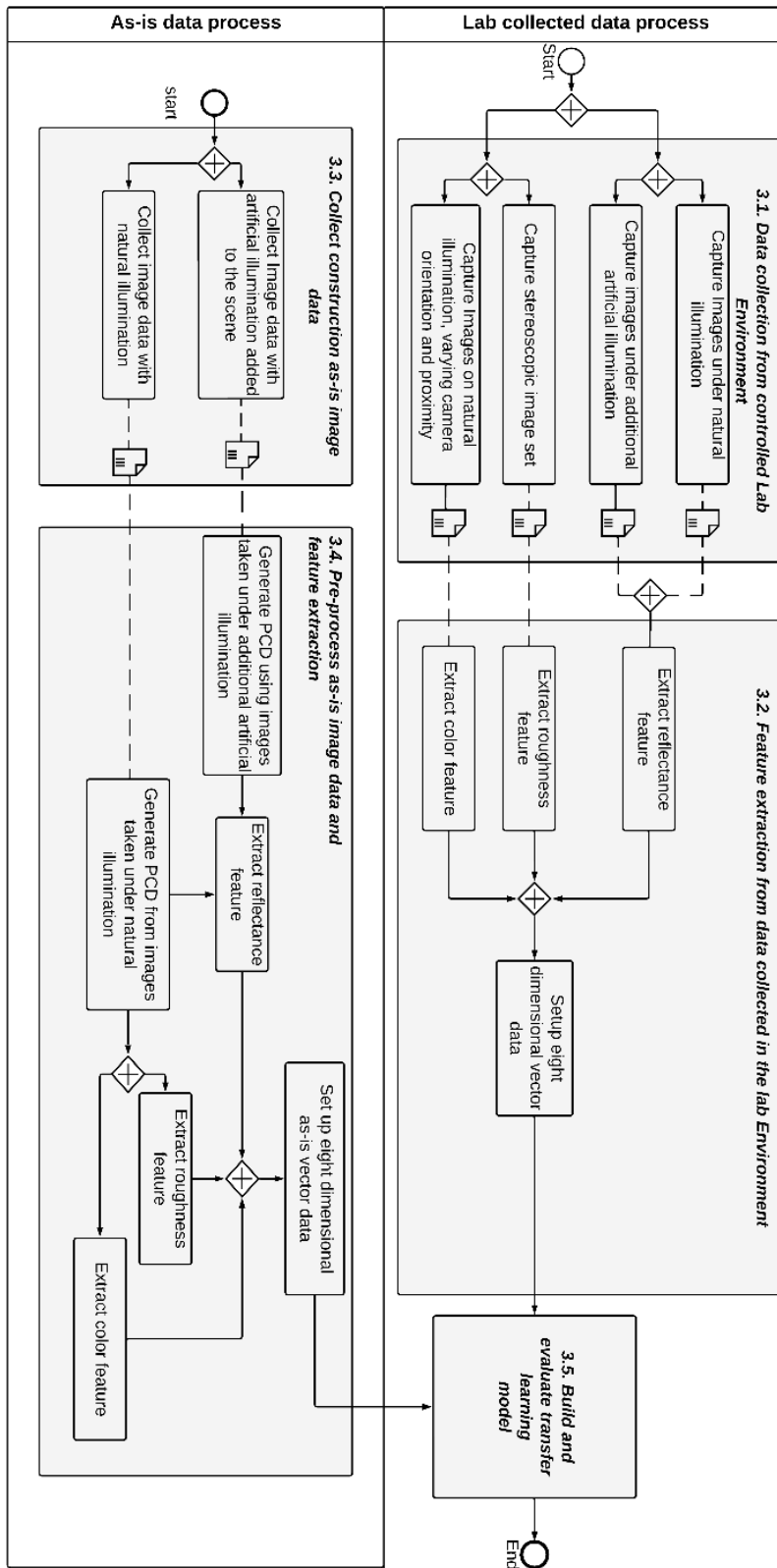

Figure 1: Proposed method

3.2.1 Extract reflectance feature

In this study, the reflectance was investigated using coupled images. The first image of each pair was taken under natural light conditions. The natural illumination in each environment could result from various light sources and be inter-refracted between solid objects, making it difficult to control the intensity and identify the amount of light originally delivered to the surface. The second set of images was taken using a controlled artificial light source (i.e., additional illumination). The natural illumination was then excluded from the captured scenes, taking the absolute difference between the couples—Figure 2(a).

The resulting image contains only the reflection of artificial light on the material surface. The resulting image was a grayscale pattern with a light glow mark—Figure 2(b). Illumination glow information was further preserved by converting the image to CIELab color space, and L-channel was taken for reflectance descriptor extraction—an illustration is shown in Figure 2(c).

As shown in Figure 2(d), a statistical analysis of maximum glow was performed on the L-channel (Figure 2(c)), and the reflectance characteristic of the material surface was defined from the difference (Figure 2(b)) between the coupled raw images (Figure 2(a)). The distribution of the glow intensity varied depending on the orientation of the artificial light source. Materials with a relatively higher reflectance surface finish resulted in more light being reflected into the camera. The brightness intensity and the size of the glow, with a value steadily decreasing to zero, are the two main measures of the reflectance feature.
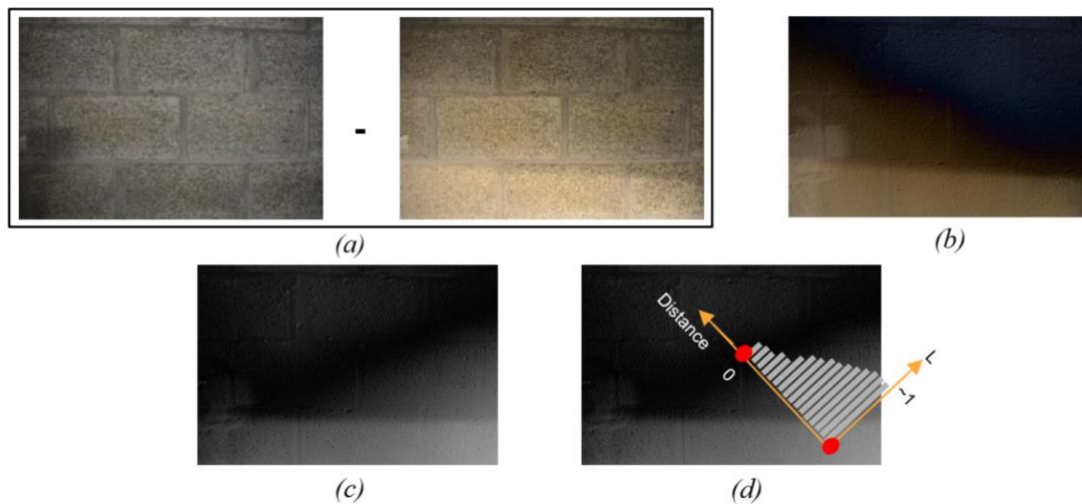

Figure 2: An illustration of coupled images.

In this study, the reflectance of a material surface was generalized using the standard deviation and mean (σ_r and $\bar{l}_r$) of the L-channel value distributions across the glow image.

3.2.2 Extract roughness feature

A 3D scene was reconstructed for each material condition by matching images using Scale Invariant Feature Transform (SIFT) image descriptor extraction (Verma and Liu, 2017) and a matching algorithm. The cluttering points were manually cropped out of the general 3D scene to keep the region of interest clean. The RANdom Sampling Consensus (RANSAC) surface-fitting algorithm (Nurunnabi et al., 2014) was used to estimate the surface. A set of points within the allowable proximity was further processed to calculate the material roughness property. Roughness was measured using the mean root square (MRS) of points distributed along the estimated point cloud surface. The normalized distribution curve of the MRS error was plotted and then taken as the roughness approximation metric. Similar to Petitpas et al. (2010), the roughness metric was represented using the standard deviation and mean parameters (σ_{Rough} and $\bar{R}$) in the training data set.

3.2.3 Extract color feature

Similarly, in the reflectance descriptor extraction process, all of the images were converted to CIELab color space to take advantage of the separability of the chrominance (Valero et al., 2019) of lightness. Moreover, Lab space is also proven to be more robust in working with slight color differences (Hamledari et al., 2017). The RGB values were converted to CIELab space, and histograms of *a* and *b* color channels were developed to represent the approximation of the color features. Similar to Valero et al. (2019), color attributes were summarized for each image in terms of standard deviation (σ_a, σ_b) and mean ($\overline{a}, \overline{b}$) values of both *a* and *b* channels.

For each material condition, the values of all three feature representations ($\sigma_r, \overline{l}_r, \sigma_a, \sigma_b, \overline{a}, \overline{b}, \sigma_{Rough}, \overline{R}$) were assembled to create an eight-dimensional vector for use as training data.

3.3 Collection of construction as-is image data

Image data were collected from various randomly-selected camera positions within the construction site. This was done to represent real conditions and allow flexibility for the collection of images. Two sets of images were collected, one under natural illumination (i.e., without altering the ambient situation during data collection) and the other with additional artificial illumination (e.g., external light sources). The two image datasets were processed independently of each other.

3.4 Pre-processing as-is image data and feature extraction

Each image frame contains multiple permanent and temporary construction members and pieces of equipment. Therefore, to detect and recognize the different material conditions, it was necessary to segment the region of interest from the image background and analyze the segmented surfaces independently. Region of interest segmentation and feature extraction can be conducted in 2D site images. However, to increase the performance of the method by reducing the effect of occlusion, image scale and distortion on the result, in this study, the as-is state of the construction is represented in 3D.

Given that it is a well-documented approach, 3D reconstruction of the site from the collected images was performed using Structure from Motion (SfM) method, in which images are matched using the SURF image matching algorithm (Li et al., 2017), and dense point cloud data were generated separately for the two distinct image sets collected under different illumination conditions.

Furthermore, RANSAC surface-fitting (Schnabel, Wahl and Klein, 2007) iterations were performed following randomly selected initiating points. Once the surfaces had been identified, points within the threshold from the fitted point were recognized as points representing each surface. Through this process, planes were segmented based on geometric proximity. However, each recognized plane contains multiple material conditions. Therefore, a patch of points that belong to the same material condition needed to be recognized.

Point cloud segmentation is beyond the scope of this paper. However, the overall process adopted to prove the methodology is presented. Point cloud pixel points were clustered into subdivisions, using the Gaussian mixture model (GMM) to achieve accurate segmentation. The GMM introduces multiple Gaussian functions fitting into the intensities of features in a data set (Jian and Vemuri, 2011). The multiple Gaussian functions were fitted on the histograms of the color attributes of the point clouds lying on a common plane. Points fitting into each Gaussian function were clustered as a separate material condition group. The process of cluster segmentation in this study was performed according to the method by Farnoosh et al. (2008).

Clustered sets of points are six-dimensional, incorporating three coordinate points and three other color attributes. Both of the image data sets collected under natural and artificial illumination were processed in a similar but distinct fashion. Features representing the condition of materials were extracted from the clustered set of point clouds. The representations were inputs for the trained algorithm to classify and label the condition in the construction site as a recognized material condition. The process of extracting reflectance, roughness, and color features from the as-is point cloud data (PCD) is described below.

Roughness:

Each cluster was fitted into a surface during the pre-processing procedure, and thus, each of the points in the cluster was within a maximum threshold of distance from the estimated plane. However, there was still a non-uniform distribution of PCD normals on the surface, depending on the orientation of the refracted incident light from the

surface into the camera lens. To estimate the irregularity in the surface, the residual values at a distance within the threshold boundary were computed for each point in a cluster. Moreover, the residual values were summarized into standard deviation and mean values (σ_{Rough} and $\overline{R}$).

Reflectance:

Two clusters of the same material condition obtained from the coupled datasets were matched by comparing their respective scene and relative geometric locations. The RGB attributes of the point cloud were converted into CIELab color space. Next, the difference between the two standard deviations and the two mean values of the CIELab L-channel obtained from the clusters of the coupled datasets was computed. The resulting values (σ_r and $\overline{l_r}$) were then registered as the reflectance measurement of the clustered material conditions.

Color:

Color feature measurement was performed on the point cloud obtained from the image dataset taken under natural light conditions. To extract the color attributes from the clustered points, the RGB attributes were converted to CIELab color space. The standard deviation and the mean of *a* and *b* color channels ($\sigma_a, \sigma_b, \overline{a}, \overline{b}$) were calculated independently and registered as color features.

Similar to the controlled lab environment data, the values of all three feature representations were assembled to create an eight-dimensional feature dataset.

3.5 Build and evaluate the model

The model developed using limited-size feature data of the lab images needs to be transferred to a new set of data generated from a separate environment using a separate process. Therefore the pre-trained model on the feature dataset from lab images needs to be fine-tuned to adopt patterns of the as-is features.

One of the available approaches that could transfer learned information from one dataset to a completely new dataset is transfer learning. Therefore, a transfer learning model was developed following the diagram in Figure 3.
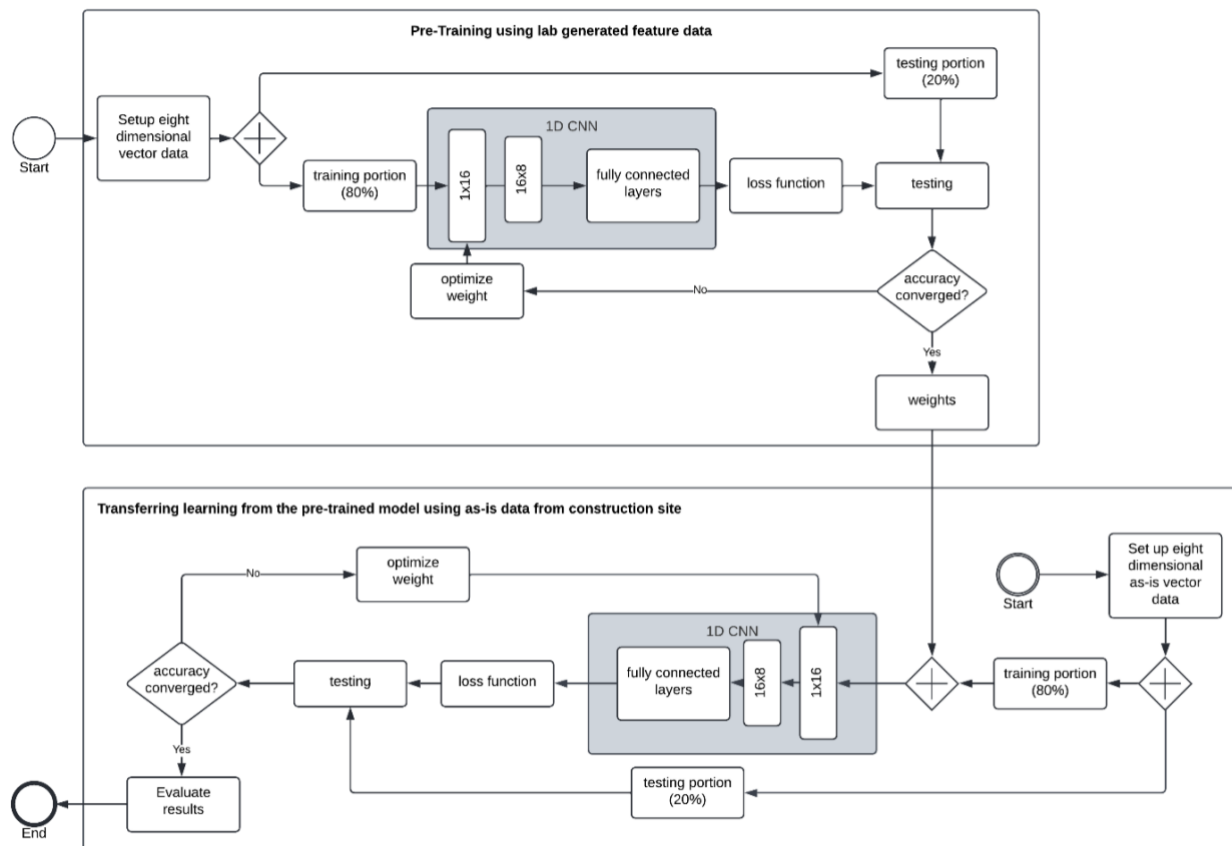

Figure 3: Build and evaluate the transfer learning model.

The model development is split into two sections, with the first being the pre-training process using the vector data extracted from the data generated in the controlled lab environment. A One-Dimensional Convolutional Neural Network (1DCNN) is developed with two layers followed by three fully connected layers. The Cross entropy loss function is used for cost computation. The eight-dimensional vector data obtained from the lab environment is split 80/20% between training and testing. The Adam optimizer is adopted to optimize backward pass weights. Once convergence is achieved, the final weights are used to start the first layer of the 1DCNN in the second section of the model development. In the second section, knowledge learned during the pre-training process is used to initiate the training of the model on the as-is data. Therefore, after obtaining the weights of the pre-trained model, the transfer learning process is conducted, where the as-is data is used to fine-tune the model.

4 DEMONSTRATION OF THE METHOD

Part of ongoing remodeling work for lab spaces at the NYU Abu Dhabi campus in Saadiyat Island, UAE, was used to test the classifying model. The selected portion of the construction site consisted of an area of approximately 76 square meters and included four different material conditions or classes. Some walls were partly gypsum-finished and partly exposed CMUs (Figure 4). The beams and columns had a smooth concrete texture, and the floor was finished with a smooth cement screed. The material condition categories (i.e., classes) are the CMUs, concrete structural members (beams/columns), gypsum-finished wall surfaces, and smooth concrete finished floors (cement screed). These classes shared similarities in certain features but could have differences in others.

In that space, we acquired images controlling significant parameters such as camera pause, the distance between the camera and the surface of the material, illumination and other camera sensor parameters such as focus, lens distorsion and light sensitivity (ISO. Images representing the real construction scenario were also collected from the construction site without controlling the environment.
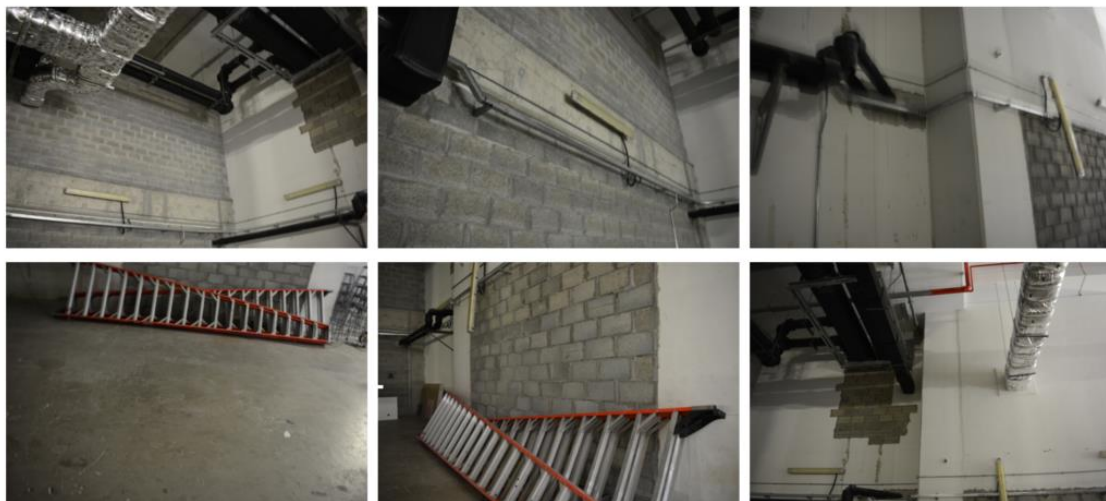

Figure 4: Material conditions of the construction site

4.1 Image data collection and processing (lab experiment)

To capture the material conditions represented by the features in the training dataset, a total of 80 images of 6,000 x 4,000 pixels size per material condition were taken using a Nikon D5200 camera of surfaces that resembled the expected conditions of the materials in the construction site. Twenty images for each material condition (i.e., class) were taken under additional artificial illumination, varying the direction and positioning of the artificial illumination source towards the target surface. Reference images to be coupled with those taken under additional artificial illumination were taken under natural illumination. Another set of 20 images was taken under natural illumination but with varying camera positions to target surface proximity and orientation. These sets of images were used to extract color information. The remaining 20 were taken with various camera orientations to create the 3D surface representation to extract roughness information. Samples of the collected raw image data are presented in Figure 5. The complete image dataset can be accessed in Mengiste et al. (2020b).

Figure 5: Sample raw image data collected to resemble the expected site material conditions.

Coupled images were deducted from each other, and the results were converted to CIELab color space. The L-channel was used to define the artificial light reflection on the material surface. Figure 6 shows the extraction of reflectance for CMUs, gypsum-finished wall, concrete structural members, and cement screed floor. These represent different conditions of materials.
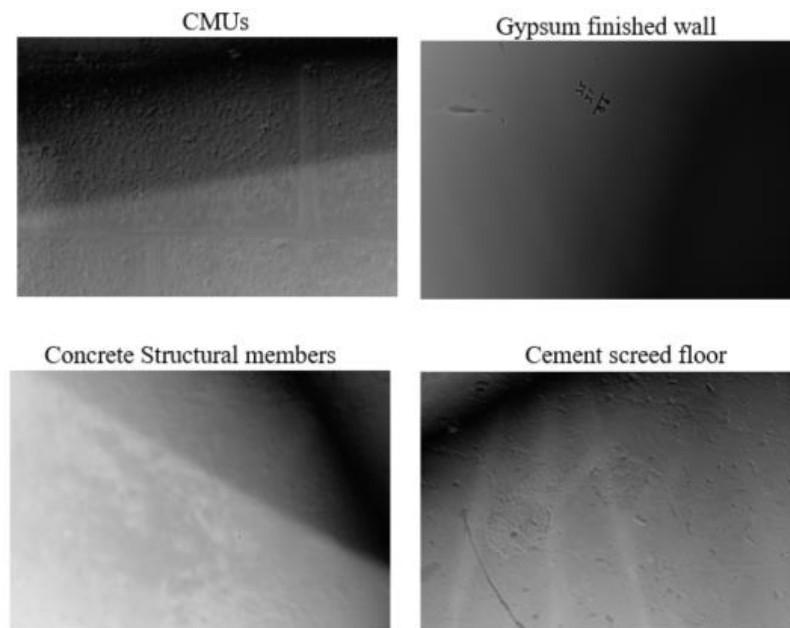

Figure 6: Extracted response to the artificial light of the four material conditions through sample images.

Figure 7(a) – (d) shows the intensity plots for multiple illumination orientations of the four material conditions. The colored lines in each graph indicate the reflectance intensity of the same material surface due to the illumination emitted from a light source placed in various orientations. The orientations considered for each surface range from +40 to -40 degrees in10 degree increments measured vertically on both sides, where zero is taken as the camera being placed exactly level with the target surface. The reflectance feature of the surface was represented as the mean and standard deviation values of each intensity plot. Image processing was performed using the OpenCV image processing library (Bradski, 2000).
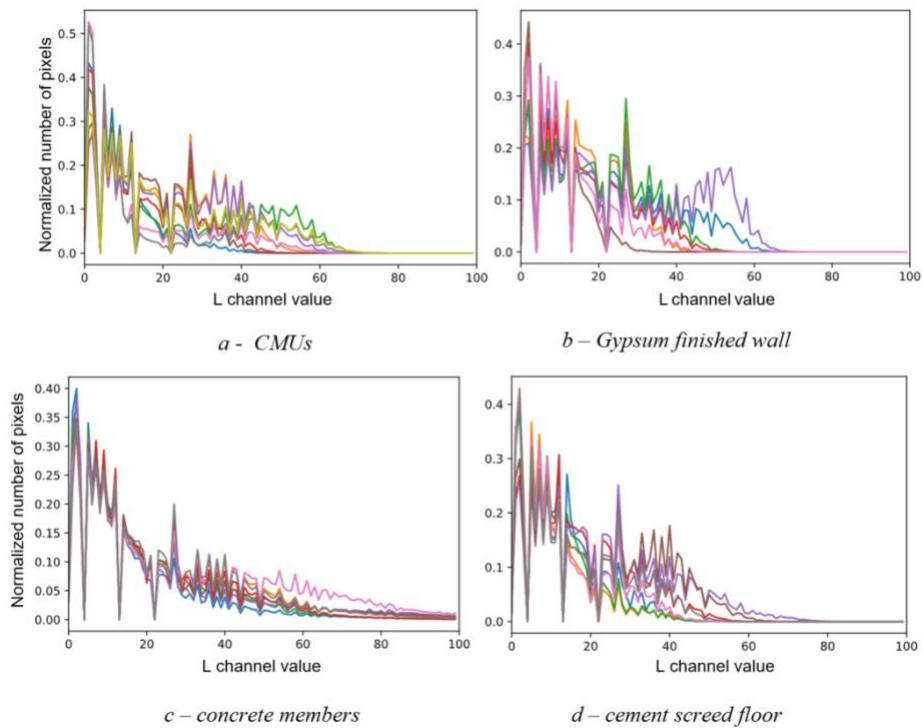
Figure 7: Light (glow) intensity plots on material surfaces.

The RGB image data collected for color feature extraction was converted to CIELab color space, and the histogram was developed for all the material conditions. Figure 8 illustrates the histograms for the *a* and *b* color channels of the four material conditions. The blue and orange color histograms show the concentration of *a* and *b* channel values, respectively. The color features were computed as the mean and standard deviation of the *a* and *b* channel intensity plots.
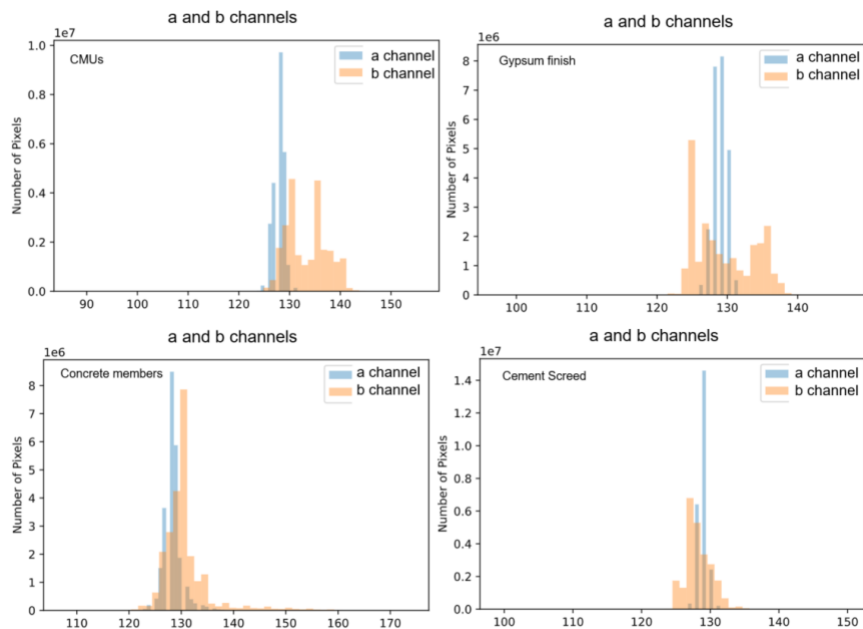

Figure 8: Examples of CIELab a and b channel histograms.

A point cloud was generated using close-up stereoscopic images of the four material conditions to compute the roughness feature. The SfM process was conducted on the image data and used the Meshroom software package (AliceVision, 2020). The PCD was further processed using Open 3D library (Zhou et al., 2018) to approximate a surface. The intensity of the geometric irregularity on the surface was computed as MRS values. The roughness values were defined as the mean and standard deviation of the MRS error distribution of each surface.

A summary of the data collection and process output is presented in Table 1. With 20 data sets for each material condition, the final classification model had 80 distinct data points, each with eight attributes. A portion of the data set is presented in Table 2, where the Class column represents CMUs as '0', Concrete structural members as '1', Gypsum finished wall as '2' and Cement screed floor as '3'.

Table 1: Summary of lab experiment database

Test	Number of images	Output
Controlled environment (lab set up) Images are taken on a controlled surface and in a predefined environment.	248 images. Where each class has 62 images composed of • 20 images - artificial illumination, varying the direction and positioning of the artificial illumination • 2 images – reference with natural illumination • 20 images - taken under natural illumination but with varying camera positions to target surface proximity and orientation. • 20 images – stereoscopic 3D surface representation	80 data points with the eight attributes (20 data points for each class).

Table 2: Portion of the feature data extracted from the images taken during the lab experiment

Material condition	i	Reflectance		Roughness (x 1000)		Color				Class
						a – channel		b – channel		
		σ_r	$\bar{l}_r$	σ_{Rough}	$\bar{R}$	σ_a	$\bar{a}$	σ_b	$\bar{b}$	
CMU wall	1	36.98	20.14	0.35	0.49	126.76	0.90	126.24	1.05	0
CMU wall	2	52.61	35.41	0.34	0.48	126.19	0.96	125.81	1.04	0
:	:	:	:	:	:	:	:	:	:	:
Concrete structural member	21	74.11	52.39	1.05	1.11	123.61	1.26	126.46	0.98	1
Concrete structural member	22	63.73	40.94	1.12	1.12	126.17	1.08	125.03	0.90	1
:	:	:	:	:	:	:	:	:	:	:
Gypsum-finished wall	41	45.63	34.13	0.52	0.49	127.90	0.92	127.02	0.27	2
Gypsum-finished wall	42	41.03	21.72	0.53	0.50	126.28	0.80	125.98	0.91	2
:	:	:	:	:	:	:	:	:	:	:
Cement screed floor	61	51.15	25.23	1.54	1.90	121.64	2.47	98.93	2.53	3
Cement screed floor	62	53.57	27.19	1.72	1.94	120.16	1.83	110.23	2.59	3
:	:	:	:	:	:	:	:	:	:	:
Cement screed floor	80	53.03	25.10	1.49	1.83	119.66	2.00	97.86	2.08	3

4.2 As-is image data collection and processing (real construction scenario)

For each case under natural and artificial lighting conditions, 130 images were collected using a Nikon D5200 camera. Complete image sets used in this section are available in a database (Mengiste et al., 2020a). As shown in Figure 5, each image frame is composed of multiple material conditions, and hence the segmentation process is conducted by generating PCD from the collected images using SfM. Coupled images are collected to measure a material's reflectance using a camera and light source, as shown in Figure 9(a-b). Image collection at the construction site was uncontrolled, with all the images taken following an arbitrary path, as shown in Figure 9(b). Figure 9(b) white dots represent the locations, and white rectangles the orientation.
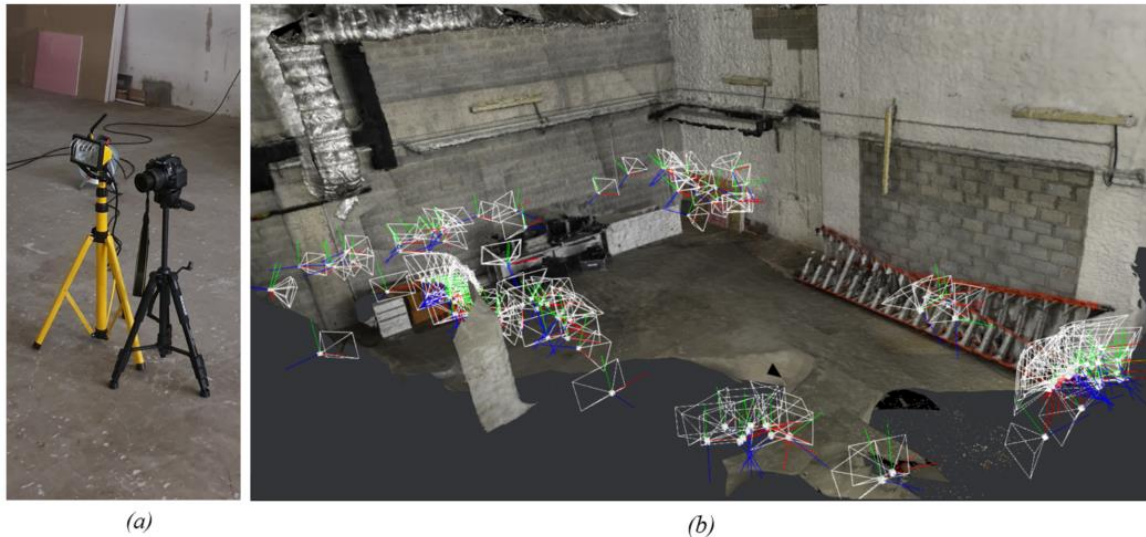
Figure 9: (a) Equipment used for data collection and (b) locations where the images were captured.

The SfM was used to reconstruct the 3D scene utilizing Meshroom software. The point clouds generated for the construction site under natural and artificial illumination are shown in Figure 10 (a) and (c), respectively. The open 3D library was used to extract surfaces based on the point geometry; RANSAC surface approximations of the segmented point clouds are shown in Figure 10 (b) and (d) for natural and artificial illumination. Different colors represent sets of PCDs that were close to the same surface.
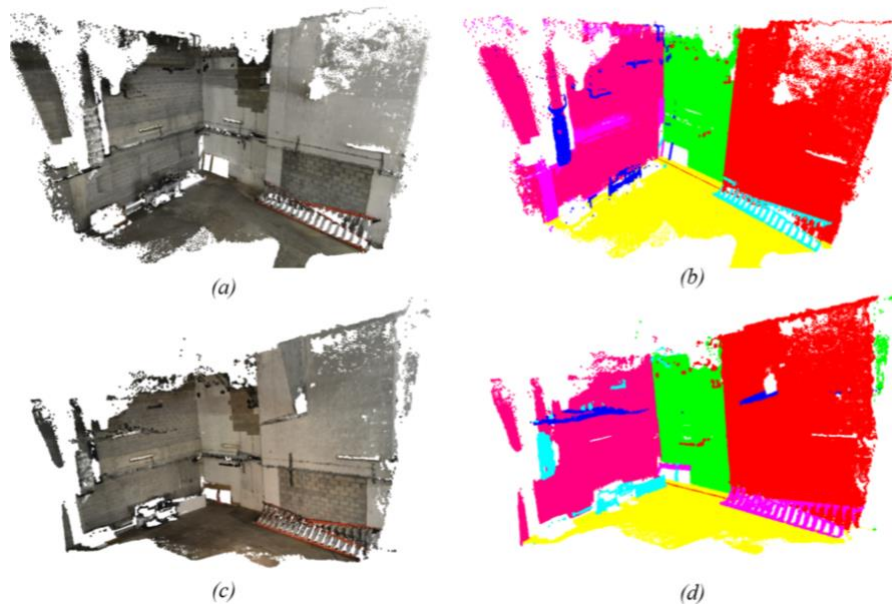

Figure 10*: (a) view of the site scene reconstruction under natural light; (b) RANSAC surface segmentation of the PCD generated from images taken under natural light; (c) view of the site scene reconstruction under artificial light; and (d) RANSAC surface segmentation of PCD generated from images taken under artificial light.*

The PCD of segmented surfaces contains RGB color values of points. The RGB values were used to compute the reflectance and color feature values. Roughness values were computed using the RMS values of the PCD of each surface cluster. Table 2 presents the summary of the data processing where out of the total of 130 x 2 images, 33 distinct feature datasets with 8 attributes were generated. The portion of the feature values extracted from the construction site scene is presented in Table 4. In clusters *(u-v)*, *u* stands for the index of the initial segment, filtered out of the total PCD using RANSAC surface fitting, and *v* represents the clustered point cloud out of the uth segment, which results from the GMM operation. In this study, GMM was performed using the Scikit-learn library (Pedregosa et al., 2011).

Table 3: Summary of real construction scenario database

Test	Number of images	Comments	Output
Real scenario (uncontrolled)	260 (130 with normal lighting + 130 with additional artificial lighting)	Images were unordered and were not controlled, i.e.,images were randomly taken without monitoring the position, and camera pause. The camera was on autofocus.	A point cloud from the images taken. From that point cloud, 33 regions/patches were selected, and the features extracted. Each patch was processed, and 33 data points were generated.

Table 4: Portion of the feature data extracted from the images taken during the real construction (as-is_ feature data)

Cluster (u-v)	Reflectance (10^{-4})		Roughness (10^{-4})		Color				Class
					a – channel (10^{-4})		b – channel (10^{-4})		
	σ_r	$\bar{l}_r$	σ_{Rough}	$\bar{R}$	σ_a	$\bar{a}$	σ_b	$\bar{b}$	
1-1	68	2896	025.9	30.7	704.3	-6400	1991	21361	1
1-2	395	2985	22.7	29.2	570.6	-6598	1422	23129	1
:	:	:	:	:	:	:	:	:	
2-1	752	4832	10.4	12.4	500.7	-8570	1204	26961	2
2-2	235	678	18.1	24.3	482.2	-8002	1491	24514	2
:	:	:	:	:	:	:	:	:	
3-1	110	2270	7.3	9.05	1127.2	-4264	2834	15422	0
3-2	434	1481	34.6	41.3	819.7	-5522	2624	17001	0
:	:	:	:	:	:	:	:	:	
4-1	382	3893	514.7	514.7	752.8	-3479	1776	14942	3
4-2	293	4036	602	697.3	731.2	-3407	1737	14283	3
:	:	:	:	:	:	:	:	:	

Finally, data from both sources were utilized to develop a classification model using the transfer learning approach.

5 RESULTS

The performance of the classification model was evaluated during the pre-training phase, using both the training and testing data portions. This is done to observe whether the model is overfitting, considering the data size. However, the model achieved 93% accuracy using the training data, close to the accuracy level obtained during the testing phase. The testing phase converged to 93% on the 142nd epoch. Similarly, the transfer-learning was evaluated with the training and testing sets. As a result, training data converged at 91% accuracy while the testing data converged at 83% accuracy. The confusion matrices Figure 11(a) and Figure 11(b) present the performance of the model when evaluated on the testing portions of pre-training and transfer learning, respectively.
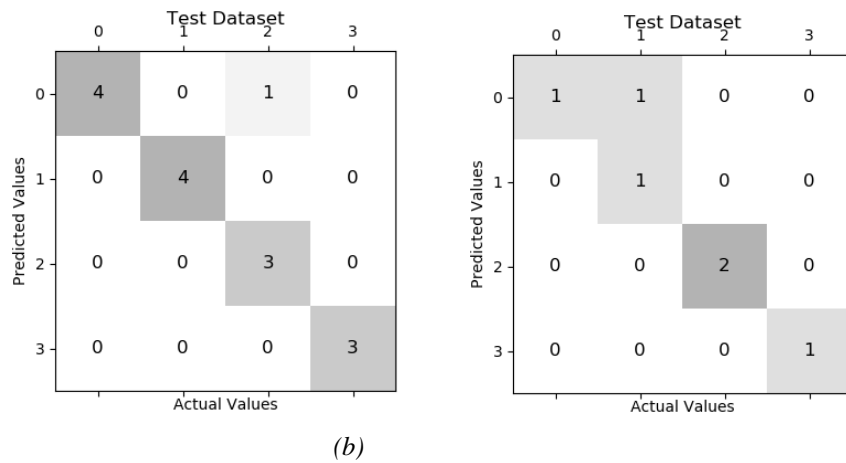
(a)   *(b)*

Figure 11: Performance of the classification model (a) Pre-trained model and (b) Transfer learning

The accuracy of the trained model was evaluated based on both specificity and sensitivity measurements. Sensitivity and specificity are measures of the rate of correctly identified positives and negatives, respectively. As shown in Table 5 and Table 6, specificity appeared to be equal to or higher than sensitivity in all the classes, except in the case of the CMUs. This is consistent in both the pre-trained model and the transfer learning. Considering all the material conditions, the transfer learning model achieved 83% accuracy with average specificity and sensitivity of 95% and 87.5%, respectively.

Table 5: Performance summary of the pre-trained model

Material condition	Class	Material	Total number of data points	Pre-trained model					
				TP	TN	FP	FN	Specificity	Sensitivity
CMUs	0	Concrete	5	4	10	1	0	0.909	1.000
Concrete members	1	Concrete	4	4	11	0	0	1.000	1.000
Gypsum	2	Gypsum	3	3	11	0	1	1.000	0.750
Cement Screed	3	Concrete	3	3	12	0	0	1.000	1.000
			15	14			Average	0.977	0.938

Table 6:Performance summary of the transfer learning model

Material condition	Class	Material	Total number of data points	Transfer learning					
				TP	TN	FP	FN	Specificity	Sensitivity
CMUs	0	Concrete	2	1	4	1	0	0.800	1.000
Concrete members	1	Concrete	1	1	4	0	1	1.000	0.500
Gypsum	2	Gypsum	2	2	4	0	0	1.000	1.000
Cement Screed	3	Concrete	1	1	5	0	0	1.000	1.000
			6	5			Average	0.950	0.875

In the case of TNs (True Negatives), a model can be considered to have correctly predicted the data point as not belonging to a class, while FP (False Positives) are instances in which the model incorrectly predicted the data point as belonging to a class. Similarly, TPs (True Positives) are the number of instances in which the data point is correctly predicted to belong to a class, while FNs (False Negatives) are incorrect predictions of not belonging to a class.

6 DISCUSSIONS

6.1 Data collection and processing

One of the challenges encountered while computing reflectance from the produced image data sets was the effect of strong shadows. A strong shadow cast on material while capturing images under artificial illumination results in a dark zone with zero pixel values. Figure 12(a) illustrates a shadow on the coupled image taken under artificial illumination. The shadow at the top corner of the first image resulted in close to zero pixel values. The pixel intensity plot illustrates the variation of illumination from 0.2 to 0.8 along the top edge of the image. Figure 12 (b) illustrates an image taken under ambient illumination.
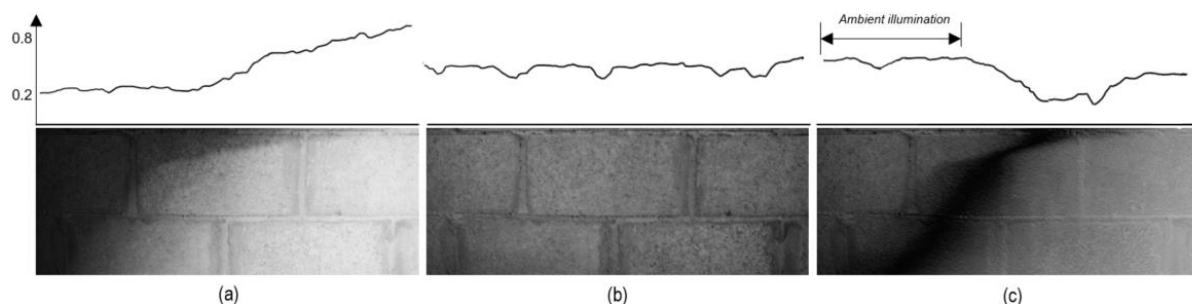

Figure 12: Effect of strong shadow

The difference between the two images in Figure 12 (a) and Figure 12 (b) is presented in Figure 12 (c). This procedure was performed to remove the effect of the ambient illumination from Figure 12 (a) and analyze the interaction of the known artificial illumination with the material surface. However, as shown in Figure 12(c), the top corner of the image resulting from the difference kept the illumination intensity value similar to Figure 12(b). The environmental illumination remained unaffected due to the shadow with zero pixel value.

6.2 Key characteristics of the classifier development

The pre-processing of the data collected in the lab converted the image into a numerical eight-dimensional vector representing three features (reflectance, roughness, and color). Each of the four material cases is represented by 20 eight-dimensional data points. Similarly, as-is image data is processed and results in a 33 x 8 feature vector. Given the database size, both in the case of pre-training and transfer learning, the hyperparameters are fine-tuned against overfitting. Figure 13(a) shows that the pre-training model has significantly improved as the learning rate changes from 0.00001 to 0.005. However, 0.0001 is taken as the optimum value considering a higher learning rate than this results in overfitting, where the perfect 100% accuracy score is registered during both training and testing.

On the other hand, in Figure 13(b), transfer learning improved inaccuracy with an increased learning rate. However, the convergence of the loss curve can only be maintained up to the learning rate of 0.0005. On the highest four learning rate values, the curve loses its consistency for epoch values higher than 40.
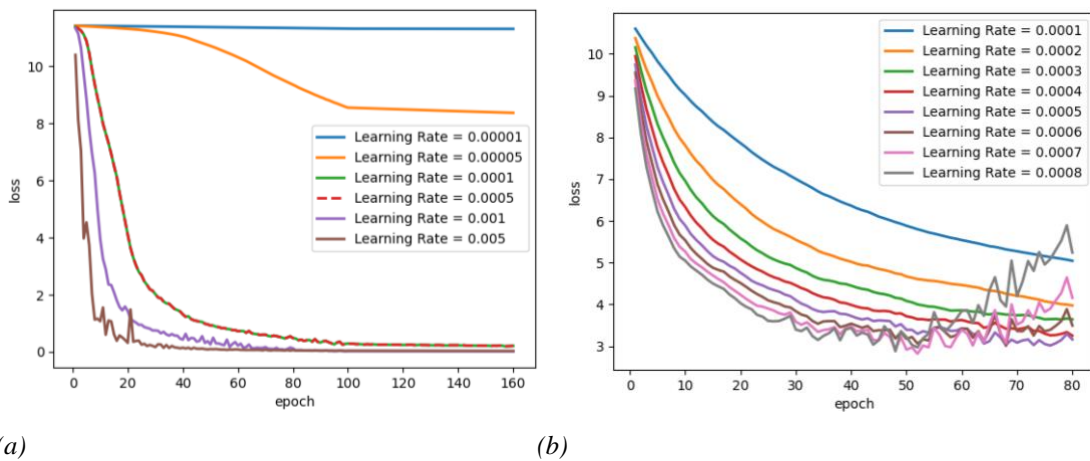

(a) *(b)*

Figure 13: Loss curves (a) Pre-training (b) Transfer learning

Taking the selected learning rate values of 0.0001 and 0.0005 for both pre-training and transfer learning, the accuracy plot is presented in Figure 14 (a) and (b). The accuracy is plotted for the training and testing data in both cases.
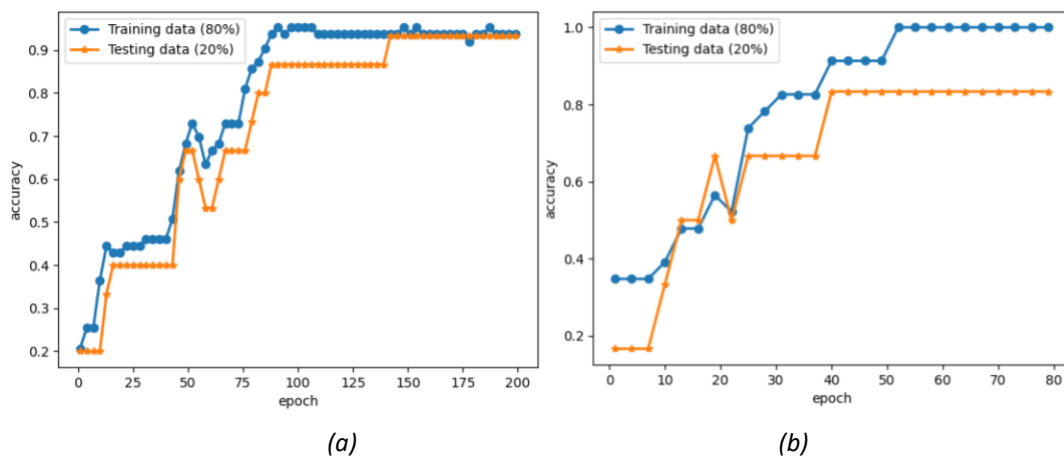

(a) *(b)*

Figure 14: (a) Accuracy curves for pre-training and (b) transfer learning

The loss (Figure 13) and accuracy (Figure 14) plots confirm that the model developed is not overfitting regardless of the data size, and the accuracy results are reliable.

6.3 Contribution to the material recognition research in construction

Based on the findings from this study, it was found that the meta-learning model is a promising alternative in construction material condition recognition where labeled data is scarce. Previously, construction material tracking research has depended on large training data sets that are not abundantly available and do not cover the whole range of construction scenarios. The performance of the handcrafted features with the classification model in this research provides evidence of its capacity to be exploited in construction material recognition research.

6.4 Practical impact

The current practice of construction material recognition is data-intensive while, developing and processing large data sets is time-consuming and computationally expensive. Moreover, detailed material conditions are overlooked, and only construction materials are recognized. Detecting and recognizing permanent and temporary material conditions can help improve the level of detail in automated tracking of construction progress and similar activities in construction that require a full understanding of the construction site.

6.5 Limitations and suggestions for future research

While deploying the recognition algorithm on-site, the data collection process includes taking pictures in ambient illumination conditions and applying artificial illumination. When there is strong sunlight on the construction site, the additional illumination is not visible, and the computational results for reflectance show no difference. Therefore, the method was tested in site conditions where the illumination of the site was relatively lower than the intensity of the artificial light. Evaluation of the proposed method for light sensitivity can be considered in future work. Moreover, given that both the lab data and the as-is data are generated from the same construction sites with a limited number of material conditions, the performance of the model when it is subjected to a dataset generated from an unseen construction site with more abundant material types and complexity is not examined.

Future work should integrate the method developed in this study with a monitoring system for progress tracking and trade productivity. The current method can be used to detect the as-is state of construction and the conditions of materials and be integrated with the planned BIM models to directly measure the amount of actual work that a specific trade has performed. The time required to cause a change in the condition of a material can be directly linked to the amount of work done. For instance, concrete curing, smoothing of rough surfaces, screeding, and plastering work usually result in textural change, while the color tone of the material remains constant. The proposed method will be extended to progress tracking in separate research.

The proposed method has demonstrated promising performance with transfer learning. However, the performance should be compared with other similar cutting-edge algorithms. Similarly, in addition to the three features adopted in this work, other feature candidates could improve the results obtained. Therefore feature optimizations and sensitivity analysis should be conducted on possible combinations of available features.

7 CONCLUSION

Construction materials possess variable color, reflectance, and roughness surface characteristics that can change throughout the progress of a construction project. This study proposes a novel method for automatic recognition of the construction material conditions on the construction site. Algorithms have been developed to extract material reflectance, roughness, and color features from image data sets. The lack of labeled data to train a machine-learning algorithm that classifies material conditions was addressed by generating a limited amount of training data using handcrafting features and taking advantage of transfer learning. The pre-trained model on the dataset obtained from the lab images attained 93% accuracy. For the actual construction site, the classification model achieved an accuracy of 83%, which can be considered favorable results given the limited dataset.

REFERENCES

AliceVision. (2020). *Meshroom: A 3D reconstruction software.* Retrieved from https://github.com/alicevision/meshroom

Bosché F. (2012). Plane-based registration of construction laser scans with 3D/4D building models. *Advanced Engineering Informatics*, *26*(1), 90–102. https://doi.org/10.1016/j.aei.2011.08.009

Bradski G. (2000). The OpenCV Library. *Dr. Dobb's Journal of Software Tools*. Retrieved from https://github.com/opencv/opencv

Braun A. et al. (2020). Improving progress monitoring by fusing point clouds, semantic data and computer vision. *Automation in Construction*, *116*, 103210. https://doi.org/10.1016/j.autcon.2020.103210

Cula O.G. and Dana K.J. (2004). 3D texture recognition using bidirectional feature histograms. *International Journal of Computer Vision*, *59*(1), 33–60. https://doi.org/10.1023/B:VISI.0000020670.05764.55

Das R. et al. (2020). Improved Feature Generalization in Smaller Datasets with Early Feature Fusion of Handcrafted and Automated Features for Content Based Image Classification. *2020 11th International Conference on Computing, Communication and Networking Technologies, ICCCNT 2020.* https://doi.org/10.1109/ICCCNT49239.2020.9225439

Deng H. et al. (2020). Automatic Indoor Construction Process Monitoring for Tiles Based on BIM and Computer Vision. *Journal of Construction Engineering and Management*, *146*(1), 04019095. https://doi.org/10.1061/(asce)co.1943-7862.0001744

Díaz-Vilariño et al. (2016). Automatic classification of urban pavements using mobile LiDAR data and roughness descriptors. *Construction and Building Materials*, *102*, 208–215. https://doi.org/10.1016/j.conbuildmat.2015.10.199

Dimitrov A. and Golparvar-Fard M. (2014). Vision-based material recognition for automated monitoring of construction progress and generating building information modeling from unordered site image collections. *Advanced Engineering Informatics*, *28*(1), 37–49. https://doi.org/10.1016/j.aei.2013.11.002

Ebner M. (2007). Color Constancy. In *Computer Vision*. Wiley.

Eismann M.T. (2012). Spectral Properties of Materials. In *Hyperspectral Remote Sensing* (pp. 133–198). https://doi.org/10.1117/3.899758.ch4

Erickson Z. et al. (2020). Multimodal material classification for robots using spectroscopy and high resolution texture imaging. *IEEE International Conference on Intelligent Robots and Systems*, 10452–10459. https://doi.org/10.1109/IROS45743.2020.9341165

Farnoosh R. et al. (2008). Image Segmentation using Gaussian Mixture Models. *IUST International Journal of Engineering Science*, *19*(1–2), 29--32.

Ghassemi N. et al. (2020). Material Recognition for Automated Progress Monitoring using Deep Learning Methods. *Computer Vision and Pattern Recognition*. Retrieved from http://arxiv.org/abs/2006.16344

Gopalakrishnan K. et al. (2017). Deep Convolutional Neural Networks with transfer learning for computer vision-based data-driven pavement distress detection. *Construction and Building Materials*, *157*, 322–330. https://doi.org/10.1016/J.CONBUILDMAT.2017.09.110

Hamledari H. et al. (2017). Automated computer vision-based detection of components of under-construction indoor partitions. *Automation in Construction*, *74*, 78–94. https://doi.org/10.1016/j.autcon.2016.11.009

Han K.K. and Golparvar-Fard M. (2014). Automated monitoring of operation-level construction progress using 4D bim and daily site photologs. *Construction Research Congress 2014: Construction in a Global Network - Proceedings of the 2014 Construction Research Congress*, 1033–1042. https://doi.org/10.1061/9780784413517.106

Hassan M.U. et al. (2017). Investigation of Terrestrial Laser Scanning Reflectance Intensity and RGB Distributions to Assist Construction Material Identification. *Proceedings of the Joint Conference on Computing in Construction (JC3)*, 507–515. https://doi.org/10.24928/jc3-2017/0312

Jian B. and Vemuri B.C. (2011). Robust point set registration using Gaussian mixture models. *IEEE Transactions on Pattern Analysis and Machine Intelligence*, *33*(8), 1633–1645. https://doi.org/10.1109/TPAMI.2010.223

Kim J. et al. (2018). RGBD Camera Based Material Recognition via Surface Roughness Estimation. *Proceedings - 2018 IEEE Winter Conference on Applications of Computer Vision, WACV 2018*, *2018-January*, 1963–1971. https://doi.org/10.1109/WACV.2018.00217

Lai Q. et al. (2020). BRDF characteristics of different textured fabrics in visible and near-infrared band. *Optics Express*, *28*(3), 3561. https://doi.org/10.1364/oe.385135

Li A. et al. (2017). An Improved FAST+SURF Fast Matching Algorithm. *Procedia Computer Science*, *107*, 306–312. https://doi.org/10.1016/j.procs.2017.03.110

Liu C. et al. (2010). Exploring features in a Bayesian framework for material recognition. *Proceedings of the IEEE Computer Society Conference on Computer Vision and Pattern Recognition*, 239–246. https://doi.org/10.1109/CVPR.2010.5540207

Liu C. and Gu J. (2014). Discriminative illumination: Per-pixel classification of raw materials based on optimal projections of spectral BRDF. *IEEE Transactions on Pattern Analysis and Machine Intelligence*, *36*(1), 86–98. https://doi.org/10.1109/TPAMI.2013.110

Mahmoudzadeh, A. et al. (2019). Estimating pavement roughness by fusing color and depth data obtained from an inexpensive RGB-D sensor. *Sensors (Switzerland)*, *19*(7). https://doi.org/10.3390/s19071655

Marschner S.R. et al. (2005). Measuring and modeling the appearance of finished wood. *ACM Transactions on Graphics*, *24*(3), 727–734. https://doi.org/10.1145/1073204.1073254

Marschner S.R. et al. (2000). Image-based bidirectional reflectance distribution function measurement. *Applied Optics*, *39*(16), 2592. https://doi.org/10.1364/ao.39.002592

Mengiste E. and Garcia de Soto B. (2018). Using the Rate of Color Evolution of a Point Cloud to Monitor the Performance of Construction Trades. *18th International Conference on Construction Applications of Virtual Reality (CONVR2018)*, (November), 345–354. Retrieved from https://www.cs.auckland.ac.nz/research/conferences/convr2018/docs/CONVR2018_proceedings.pdf

Mengiste E. et al. (2020a). *As-is image dataset for testing*. Retrieved from http://bit.ly/3bxJDqn%0A

Mengiste E. et al. (2020b). *Laboratory image dataset for training*. Retrieved from http://bit.ly/3t3h0aA%0A

Nurunnabi A. et al. (2014). Robust statistical approaches for local planar surface fitting in 3D laser scanning data. *ISPRS Journal of Photogrammetry and Remote Sensing*, *96*, 106–122. https://doi.org/10.1016/j.isprsjprs.2014.07.004

Ohi A.Q. et al. (2021). FabricNet: A fiber recognition architecture using ensemble convnets. *IEEE Access*, *9*, 13224–13236. https://doi.org/10.1109/ACCESS.2021.305198019

Pedregosa F. et al. (2011). Scikit-learn: Machine Learning in Python. In *Journal of Machine Learning Research* (Vol. 12). Retrieved from http://scikit-learn.sourceforge.net.

Petitpas B. et al. (2010). Roughness measurement from multi-stereo reconstruction. *International Archives of the Photogrammetry, Remote Sensing and Spatial Information Sciences - ISPRS Archives*, *38*. Retrieved from http://www.ltci.enst.fr

Pulse of the Profession. (2021). *Beyond Agility*. Retrieved from https://www.pmi.org/-/media/pmi/documents/public/pdf/learning/thought-leadership/pulse/pmi_pulse_2021.pdf?v=b5c9abc1-e9ff-4ac5-bb0d-010ea8f664daandsc_lang_temp=en

Quintana B. et al. (2018). Door detection in 3D coloured point clouds of indoor environments. *Automation in Construction*, *85*, 146–166. https://doi.org/10.1016/j.autcon.2017.10.016

Schnabel R.et al. (2007). Efficient RANSAC for point-cloud shape detection. *Computer Graphics Forum*, *26*(2), 214–226. https://doi.org/10.1111/j.1467-8659.2007.01016.x

Shorten C. and Khoshgoftaar T.M. (2019). A survey on Image Data Augmentation for Deep Learning. *Journal of Big Data*, *6*(1), 1–48. https://doi.org/10.1186/S40537-019-0197-0/FIGURES/33

Sole A. et al. (2018). Evaluating an image-based bidirectional reflectance distribution function measurement setup. *Applied Optics*, *57*(8), 1918. https://doi.org/10.1364/ao.57.001918

Son H. et al. (2012). Automated Color Model–Based Concrete Detection in Construction-Site Images by Using Machine Learning Algorithms. *Journal of Computing in Civil Engineering*, *26*(3), 421–433. https://doi.org/10.1061/(ASCE)CP.1943-5487.0000141

Son H. et al. (2014). Classification of major construction materials in construction environments using ensemble classifiers. *Advanced Engineering Informatics*, *28*(1), 1–10. https://doi.org/10.1016/j.aei.2013.10.001

Teizer J. (2015). Status quo and open challenges in vision-based sensing and tracking of temporary resources on infrastructure construction sites. *Advanced Engineering Informatics*, *29*(2), 225–238. Retrieved from https://doi.org/10.1016/j.aei.2015.03.006

Valero E. et al. (2019). Automated defect detection and classification in ashlar masonry walls using machine learning. *Automation in Construction*, *106*(December 2018), 102846. https://doi.org/10.1016/j.autcon.2019.102846

Verma A. and Liu C. (2017). SIFT features in multiple color spaces for improved image classification. In *Intelligent Systems Reference Library* (Vol. 121, pp. 145–166). https://doi.org/10.1007/978-3-319-52081-0_7

Weiss K. et al. (2016). A survey of transfer learning. *J Big Data.*, *3*(1), 9. https://doi.org/10.1186/s40537-016-0043-6

Zhang C. and Arditi D. (2013). Automated progress control using laser scanning technology. *Automation in Construction*, *36*, 108–116. https://doi.org/10.1016/j.autcon.2013.08.012

Zhang H. et al. (2015). Reflectance hashing for material recognition. *Proceedings of the IEEE Computer Society Conference on Computer Vision and Pattern Recognition*, *07-12-June*, 3071–3080. https://doi.org/10.1109/CVPR.2015.7298926

Zhou Q.-Y. et al. (2018). *Open3D: A Modern Library for 3D Data Processing*. Retrieved from http://arxiv.org/abs/1801.09847